ANESTHESIOLOGY

Mast Cell Degranulation and Fibroblast Activation in the Morphine-induced Spinal Mass

Role of Mas-related G Protein-coupled Receptor Signaling

Tony L. Yaksh, Ph.D., Kelly A. Eddinger, B.S., R.V.T., Shinichi Kokubu, M.D., Ph.D., Zhenping Wang, Ph.D., Anna DiNardo, M.D., Ph.D., Roshni Ramachandran, Ph.D., Yuelian Zhu, Ph.D., Yajun He, M.D., Fieke Weren, M.S., Daphne Quang, B.S., Shelle A. Malkmus, B.S., R.V.T., Katherine Lansu, Ph.D., Wesley K. Kroeze, Ph.D., Brian Eliceiri, Ph.D., Joanne J. Steinauer, B.S., Peter W. Schiller, Ph.D., Peter Gmeiner, Ph.D., Linda M. Page, Pharm.D., Keith R. Hildebrand, D.V.M.

ANESTHESIOLOGY 2019; 131:132–47

EDITOR'S PERSPECTIVE

What We Already Know about This Topic

- The formation of intrathecal masses complicates the use of intrathecal opioid therapy for chronic pain
- The degranulation of mast cells has been linked to intrathecal mass formation

What This Article Tells Us That Is New

- Using a guinea pig model, masses formed around intrathecal catheters when morphine was infused, and this mass formation was not prevented by opioid receptor blockade
- Non-opioid receptor mediated stimulation of Mas-related G protein-coupled receptor appeared to be mechanism responsible for mast cell degranulation, fibroblast proliferation and ultimately mass formation
- Agents not activating Mas-related genes at analgesic doses did not produce masses

ABSTRACT

Background: As the meningeally derived, fibroblast-rich, mass-produced by intrathecal morphine infusion is not produced by all opiates, but reduced by mast cell stabilizers, the authors hypothesized a role for meningeal mast cell/fibroblast activation. Using the guinea pig, the authors asked: (1) Are intrathecal morphine masses blocked by opiate antagonism?; (2) Do opioid agonists not producing mast cell degranulation or fibroblast activation produce masses?; and (3) Do masses covary with Mas-related G protein-coupled receptor signaling thought to mediate mast cell degranulation?

Methods: In adult male guinea pigs (N = 66), lumbar intrathecal catheters connected to osmotic minipumps (14 days; 0.5 μl/h) were placed to deliver saline or equianalgesic concentrations of morphine sulfate (33 nmol/h), 2',6'-dimethyl tyrosine-(Tyr-D-Arg-Phe-Lys-NH2) (abbreviated as DMT-DALDA; 10 pmol/h; μ agonist) or PZM21 (27 nmol/h; biased μ agonist). A second pump delivered subcutaneous naltrexone (25 μg/h) in some animals. After 14 to 16 days, animals were anesthetized and perfusion-fixed. Drug effects on degranulation of human cultured mast cells, mouse embryonic fibroblast activation/migration/collagen formation, and Mas-related G protein-coupled receptor activation (PRESTO-Tango assays) were determined.

Results: Intrathecal infusion of morphine, DMT-DALDA or PZM21, but not saline, comparably increased thermal thresholds for 7 days. Spinal masses proximal to catheter tip, composed of fibroblast/collagen type I (median: interquartile range, 0 to 4 scale), were produced by morphine (2.3: 2.0 to 3.5) and morphine plus naltrexone (2.5: 1.4 to 3.1), but not vehicle (1.2: 1.1 to 1.5), DMT-DALDA (1.0: 0.6 to 1.3), or PZM21 (0.5: 0.4 to 0.8). Morphine in a naloxone-insensitive fashion, but not PZM21 or DMT-DALDA, resulted in mast cell degranulation and fibroblast proliferation/collagen formation. Morphine-induced fibroblast proliferation, as mast cell degranulation, is blocked by cromolyn. Mas-related G protein-coupled receptor activation was produced by morphine and TAN67 (∂-opioid agonist), but not by PZM21, TRV130 (mu biased ligand), or DMT-DALDA.

Conclusions: Opiates that activate Mas-related G protein-coupled receptor will degranulate mast cells, activate fibroblasts, and result in intrathecal mass formation. Results suggest a mechanistically rational path forward to safer intrathecal opioid therapeutics.

(ANESTHESIOLOGY 2019; 131:132–47)

The pivotal role played by spinal systems in the encoding of information relevant to the expression of pain is nowhere more evident than the selective attenuation of the response to strong and/or tissue-damaging stimuli induced by intrathecal opioids. This action is mediated by opioid receptors on nociceptive primary afferents and second order

This article is featured in "This Month in Anesthesiology," page 1A. Supplemental Digital Content is available for this article. Direct URL citations appear in the printed text and are available in both the HTML and PDF versions of this article. Links to the digital files are provided in the HTML text of this article on the Journal's Web site (www.anesthesiology.org). This article has a video abstract. Portions of this work were presented at the North American Neuromodulation Society meeting in Las Vegas, Nevada, January 11-14, 2018.

From the Laboratory of Anesthesiology Research, Department of Anesthesiology (T.L.Y., K.A.E., S.K., R.R., Y.Z., Y.H., F.W., D.Q., S.A.M., J.J.S.), Department of Dermatology (Z.W., A.D.), and Division of Trauma, Department of Surgery (B.P.E.), University of California, San Diego, California; the Department of Pharmacology, University of North Carolina-Chapel Hill, Chapel Hill, North Carolina (K.L., W.K.K); Montreal Clinical Research Institute and the Department of Pharmacology and Physiology, University of Montreal, Quebec, Canada (P.W.S.); Department of Chemistry and Pharmacy, Friedrich-Alexander University Erlangen-Nurnberg, Erlangen, Germany (P.G.); and Implantables Research and Technology, Medtronic, Inc., Restorative Therapies Group, Minneapolis, Minnesota (L.M.P., K.R.H.).

 Anesthesiology 2019; 131:132–47. DOI: 10.1097/ALN.0000000000002730

dorsal horn neurons.[1,2] Development of chronic implantable spinal delivery systems allowed continuous intrathecal opioid infusion as a chronic pain therapy.[3]

The observation that patients receiving intrathecal opioids displayed neurologic signs secondary to local spinal cord compression was not reported in humans until 1991,[4,5] and then recapitulated in dogs,[6] sheep,[7] and guinea pigs.[8] Preclinical work emphasized that this compression resulted from a fibroblast-rich mass in a collagen matrix arising from the dura-arachnoid adjacent to the delivery site.[6,8,9]

The intrathecal mass has several defining properties: (1) it is produced by several opioids (*e.g.*, morphine, hydromorphone), but not others (*e.g.*, fentanyl and alfentanil)[10,11]; and (2) formation in dogs is not prevented by opioid antagonism. These observations support the argument that these effects parallel the pharmacology of mast cell degranulation and are not mediated by an opioid receptor.[12] Meningeal mast cells are indeed degranulated in a naloxone-independent fashion by morphine.[11] The role of mast cell degranulation in intrathecal morphine-induced mass formation is supported by the observation that mast cell stabilizers could reduce the incidence or size of the intrathecal mass in dog.[9] Accordingly, we hypothesized that the mass is produced by degranulation of meningeal mast cells, releasing agents that stimulate fibroblastic activity and collagen deposition,[8] or by a direct effect upon fibroblast proliferation and migration.[13] Degranulation of mast cells by morphine is mediated by a family of Mas-related G protein-coupled receptors.[14,15] This leads to the hypothesis that agents activating Mas-related genes will produce mast cell degranulation and intrathecal masses, while conversely, this effect will be absent in opiates that neither activate Mas-related genes nor degranulate mast cells.

The present studies address three questions using the guinea pig intrathecal model.[8] (1) Does opioid antagonism prevent morphine-evoked masses in a second species? (2) Do opioid agonists showing reduced mast cell degranulation or fibroblast activation show reduced mass formation at equianalgesic concentrations? (3) Does the mast cell degranulating effect, the effects upon fibroblast proliferation, and the ability to activate Mas-related genes covary with the propensity of a specific opioid to yield an intrathecal mass? Recent work demonstrates that the mu-opioid agonist morphine activates Mas-related genes and results in degranulation of mast cells.[15] Conversely, PZM21, developed as a biased μ-opioid ligand, fails to activate Mas-related genes and, as we show here, will not degranulate mast cells or produce a spinal mass. Alternatively, mu-opioid ligands such as the dermorphin-derived peptides (2',6'-dimethyl tyrosine-[Tyr-D-Arg-Phe-Lys-NH2], abbreviated as DMT-DALDA) are extremely potent after intrathecal delivery,[16,17] and while they degranulate mast cells, we show here that the low concentrations required to produce mu-opiate receptor–mediated analgesia fails to produce a mass *in vivo*.[18,19]

Material and Methods

These studies were carried out according to a protocol approved by the Institutional Animal Care and Use Committee at the University of California, San Diego, California.

In-life Studies

Animals. Adult male Hartley guinea pigs (250 to 275 g) were purchased from Charles River Labs (USA). Animals were pair-housed in standard cages and maintained on a 12:12-h light–dark cycle. After a minimum of 2 days of acclimation, animals were prepared with chronic lumbar intrathecal catheters. For continuous infusion, the catheter was connected to subcutaneously implanted osmotic minipumps (Alzet model 2002; DURECT Corporation, USA). Guinea pig chow and water were freely available. All procedures and testing were conducted during the daylight cycle.

Behavioral Testing. Guinea pigs were randomly selected for study and prepared with preloaded intrathecal catheters and pumps. Before initiation of drug delivery, baseline behavioral and testing data were taken. At selected times after the initiation of infusion of the test or control article, data were collected again. All nociceptive and behavioral assessments were made with observers blinded as to the pump contents. Behavioral data review and analysis were performed after the completion of the histologic assessments.

(1) *Acute Thermal Escape.* To assess hind paw thermal escape, a Hargreaves-type hind paw thermal stimulator system was used[20] (Torrey Pines Instruments, USA). This system directed a focused light beam on the plantar surface of the paw, through a glass plate upon which the guinea pig stood. Surface temperature was maintained at 28°C. The guinea pigs were placed in the thermal escape box and allowed to acclimate for approximately 30 min before testing. A brisk withdrawal of the paw was taken as the response. Lack of a response within 20 s was cause to terminate the test and assign the score of "20 s." A latency measurement was taken for the right and left hind paws and averaged for the analysis datum. Latency assessments were then made at intervals before and after initiation of drug delivery.

(2) *Motor Assessment.* Motor assessments included: righting response, symmetrical ambulation, and hind paw proprioceptive function (return of paw to normal position after placing the dorsum of the paw on a horizontal surface). All assessments were noted as "present," "absent," "within normal limits," or "abnormal."

(3) *Behavioral Assessment.* General behavioral assessments were made during each period of observation and specifically included: corneal reflex, pinna reflex, scratching and motor assessment. For analysis, the mean ± SEM of the thermal escape latencies were plotted *versus* time. To facilitate comparisons between groups, data for each animal were converted to area under the curve where the escape latency data were converted to percent of the maximum possible effect (%MPE = [Test value T_x − T_0 value]/[Cutoff value − 20 s − T_0 value]) × 100. The area under

the percent of the maximum possible effect curve was then calculated for each animal. Motor assessment included: righting response, symmetrical ambulation, and hind paw proprioceptive function (return of paw to normal position after placing the dorsum of the paw on a horizontal surface). All assessments were noted as "present," "absent," "within normal limits," or "abnormal."

Surgical Preparation. Animals were prepared following aseptic precautions with lumbar intrathecal catheters and connected to osmotic minipumps. This procedure and the construction of the associated catheter are explicitly detailed elsewhere.[8] In brief, the polyurethane intrathecal catheter was constructed from polyurethane (polyurethane 10 0.13-mm inside diameter/0.27-mm outside diameter), and the external component was polyurethane (polyurethane 27 0.40-mm inside diameter/0.70-mm outside diameter) (Instech Laboratories, Inc., USA). An additional short piece of polyurethane tubing (polyurethane 40: 0.60-mm inside diameter/1.0-mm outside diameter) was fitted to allow connection to the osmotic pump. All were joined by a bonding agent (thin instant adhesive gap fill, 0.001–0.003 inches; Scientific Commodities, USA). A stainless steel Teflon-coated stylet (0.003 ± 0.0003 × 73 inches, EZ Grind process; Wytech Industries, Inc., USA) was fed into the catheter lumen. Each catheter was individually packaged, and ethylene oxide sterilized. For catheter placement, guinea pigs were sedated (ketamine: 20 mg/kg, intraperitoneal; xylazine: 2 mg/kg, intraperitoneal) and the back of the neck shaved and surgically prepped. The animal was placed in a rodent stereotaxic head holder and anesthesia maintained by delivery of oxygen and isoflurane (2%) through a fitted face mask. Animals were monitored during the procedure to ensure adequate anesthetic depth. The catheter was inserted through an incision in the atlantooccipital membrane following exposure by incision and blunt dissection and passed 11.5 cm caudally to the T13-L1 spinal segment. For continuous infusion, the catheter was tunneled caudally to a site on the upper back, where a subcutaneous incision was made, and a small pocket was dissected to hold the osmotic mini pump. The catheter was then connected. The wound was sutured in layers. Upon terminating the anesthesia, a subcutaneous bolus of lactated Ringer's (1 ml/50 g bodyweight) was given between the scapulae. An injection of Rimadyl (5 mg/kg, subcutaneous; Zoetis Inc., USA) was always given for postoperative analgesia. Average duration of the implant procedure was 20 to 30 min.

Drugs

In Vivo. The following drugs were employed for intrathecal delivery. Morphine was prepared from commercially available, preservative-free morphine sulfate for intrathecal use (morphine sulfate injection, MW: 379 Da; USP 25 mg/ml, preservative free; Hospira, Inc., USA). The μ agonist DMT-DALDA ([H-Dmt-D-Arg-Phe-Lys-NH2; Dmt. 2',6'-dimethyltyrosine] MW: 981 Da) was synthesized as previously described.[19] The biased μ ligand PZM21 (MW: 362 Da) was synthesized as previously described.[15] All solutions were diluted and prepared using preservative-free sterile saline for injection (0.9% sodium chloride injection, United States Pharmacopeia; Hospira, Inc.). The sodium chloride package insert lists the pH between 4.5 and 7.0.

Ex Vivo. For the *ex vivo* studies with mast cells and fibroblasts, morphine, PZM21 and DMT-DALDA, and fentanyl were employed. In addition, to assess Mas-related G protein-coupled receptor-X activation in the PRESTO-Tango assays, additional drugs were employed, including: TAN67 (a potent δ-opioid agonist: *R*⋆,*S*⋆)-(±)-2-Methyl-4aa-(3-hydroxyphenyl)-1,2,3,4,4a,5,12,12aa-octahydroquinolino [2,3,3-*g*]isoquinoline dihydrobromide: MW: 387 Da; Sigma; Cat. no. T5824) and TRV 130 (a biased μ-opioid agonist; MW: 344 Da; courtesy Bryan Roth, M.D., Ph.D., Department of Pharmacology, University of North Carolina, Chapel Hill, North Carolina); mitiglinide (MW: 315 Da; Sigma Cat. no. SML0234) serves as positive control for Mas-related gene activation, deoxycholic acid (MW: 393 Da; Sigma Cat. no. D2510) is a partial Mas-related gene agonist, and cromolyn sodium (MW = 468 Da; Sigma Cat. no. C0399) was assessed for its ability to activate Mas-related genes or antagonize the effects of Mas-related gene agonists.

Study Groups. In the current studies, guinea pigs were randomly selected from their group-housed cages to receive infusion pumps prepared to deliver 0.5 μl/h for 14 days of one of the following formulated drugs: vehicle (0.9% NaCl), morphine sulfate (25 mg/ml: 66 nmol/μl), PZM21 (20 μg/μl: 20.4 nmol/μl), or DMT-DALDA (19.6 ng/μl: 20 pmol/μl). To determine the effects of systemic opioid antagonism on spinal mass formation, a second pump was also placed subcutaneously to deliver naltrexone HCl (50 mg/ml: 25 μg/h; approximately 75 $\mu g \cdot kg^{-1} \cdot h^{-1}$ for 14 days; Sigma-Aldrich, USA) in a group of animals receiving intrathecal morphine. The concentration of morphine employed in this study was based on previous work in this model.[8] The concentrations of DMT-DALDA and PZM21 employed in the current studies, which were equiactive to morphine, were determined in preliminary concentration ranging studies with intrathecal infusion in intrathecal catheterized adult male Sprague-Dawley rats using osmotic pumps (unpublished data).

Histologic Procedures for Tissue Harvest. For tissue harvest, guinea pigs were deeply anesthetized with isoflurane anesthetic and given a 1.0 ml intraperitoneal injection of Beuthanasia-D (euthanasia solution consisting of phenytoin/pentobarbital; Intervet/Schering-Plough Animal Health Corp., USA). They were then transcardially perfused with 1 ml/g of body weight of heparinized saline followed by 1 ml/g of body weight of 4% paraformaldehyde in 0.1 M phosphate buffer. Spinal columns were harvested and underwent decalcification for 3 to 5 days at room temperature using Immunocal bone decalcifier (American MasterTech

Scientific, Inc., USA). After decalcification was complete, the spinal column was blocked *via* a template; block A (cervical), B (thoracic), and C1, C2, C3, C4 (lumbar/sacral) placed in tissue cassettes and processed to paraffin. Paraffin blocks were sectioned at 5 to 10 μm using a rotary microtome (Leica 2135, Leica Biosystems, Germany), and sections were slide mounted. Slides were stained with hematoxylin and eosin and Picro-Sirius for collagen. Hematoxylin and eosin staining was performed using Gills Hematoxylin #2 and Eosin Y alcoholic (Sigma Millipore, USA). Hematoxylin and eosin images were captured using an Olympus BX51 microscope (Olympus, USA) and Lumenera Infinity 3S camera with Infinity Analyze software (Lumenera Corporation, Canada). Picro-Sirius collagen staining was performed following the manufacturer's protocol (American MasterTech Scientific, Inc., USA). Picro-Sirius bright field and polarized birefringence images were captured on a Nikon Eclipse 80i microscope with Nikon DS-Fi1 camera and Digital Sight DS-L2 software system (Nikon Inc., USA). When viewed under polarized light, Picro-Sirius stained sections showed thick (yellow-orange birefringence) and thin (green birefringence) collagen fibers, respectively, of types 1 and 3 collagen.[21,22]

Histologic Assessment. For pathology assessment, all animals submitted for tissue harvest were analyzed. If the catheter penetrated the cord, the presence of the parenchymal catheter was noted, but no score was given. Two quantification approaches were employed, as previously described.[8] In brief, three reviewers independently, and without knowledge of treatment, first assigned a pathology grade (0 to 4) to each animal based on criteria previously outlined. Second, each reviewer performed a forced ranking of all representative sections from least to most severe and each animal was then assigned the rank given to them by the reviewer. In each case, the mean of the three pathology scores or ranks was assigned to that animal. The score and ranking for each animal were then presented as scatter plots by treatment and used in the subsequent comparisons of treatment effects.

Ex Vivo Studies

Mast Cells. LAD2, a bone marrow-derived human mast cell line,[23] was cultured in StemPro-34 serum-free medium with StemPro-34 Nutrient Supplement (Gibco, USA), l-glutamine (2 mM; Gibco), penicillin (100 U/ml)/streptomycin (100 μg/mL; Gibco), and 100 ng/ml recombinant human stem cell factor (R&D Systems, Inc., USA). Half of the media was replaced weekly by adding an equal volume of fresh StemPro-34 containing 100 ng/ml recombinant human stem cell factor. Well concentrations were maintained between 0.25 to 0.5 × 10^6 cells/ml to minimize clumping.[24] Degranulation was assessed by measuring the activity of β-hexosaminidase in the supernatants[25] of 5 × 10^5 LAD2 cells in 200 μl saline phosphate buffer (0.9% NaCl, 10 mM NaH_2PO_4, 45 mM glucose), incubated for 2 h with the test agents (morphine, DMT-DALDA, and PZM21). For each sample assayed, cell supernatant aliquots (20 μl) were mixed with substrate solution (100 μl: 1 mM 4-methylumbelliferyl-2-acetamide-2-deoxy-β-D-glucopyranoside; EMD Millipore, USA) in 0.1 M sodium citrate buffer (pH 4.5), and were incubated for 2 h at 37°C in the dark. Reaction was stopped by addition of 12 μl of 0.2 M glycine (pH 10.7). Reaction mixtures were excited at 365 nm and measured at 460 nm in a fluorescence plate reader (Gemini EM microplate spectrofluorometer; Molecular Devices, USA). To determine the total cellular content of this enzyme, an equivalent number of cells were lysed with 1% triton X-100 (Sigma Aldrich, USA). Release of β-hexosaminidase was calculated as the percentage of the total enzyme content. Compound 48/80 was used to promote complete mast cell degranulation in an IgE-independent way.[26]

Mouse Embryonic Fibroblasts. Mouse embryonic fibroblasts were obtained from ATCC (#CRL-2214). Mouse embryonic fibroblasts were cultured in 75-cm^2 culture flask in 1X Dulbecco's Modified Eagle Medium supplemented with 10% non–heat inactivated fetal bovine serum, 1% penicillin/streptomycin, 1% sodium pyruvate (100 mM), 1% Glutamax 100X, and 1% minimal essential medium nonessential amino acids 100X (Thermo Fisher Scientific, USA) and incubated at 37°C in a humidified 5% CO_2 environment. Mouse embryonic fibroblasts were grown to a 70 to 90% confluence before the next passage or for experiments. Cells were passaged by trypsinization, with 0.25% trypsin EDTA 1X (Thermo Fisher Scientific). Cells at passages 2 to 20 were used for the experiments.

Proliferation Assay. To assess proliferation of mouse embryonic fibroblasts, cells were detached from the flask and centrifuged and rehydrated in the growing media. The cells were then seeded at a density of 2 × 10^4 cells per well in a 12-well plate and incubated for 24 h, after which mouse embryonic fibroblasts were incubated with morphine sulfate (0.3 nM to 300 μM), fentanyl (0.3 pM to 300 nM), naloxone (3 μM), DMT-DALDA (0.3 nM to 30 μM), or PZM21 (0.03 μM - 30 μM) for 48 h at 37°C. The control group was incubated with the medium alone. The effect of drug on cell proliferation was determined by counting the number of cells in each well using hemocytometer by the observer blinded to the treatment.

Migration Assay. In a limited assessment of the effects of morphine on fibroblast migration, mouse embryonic fibroblasts were plated onto the top of transwell plates (50 K · $well^{-1}$ · 200 μl^{-1}), precoated with collagen (1 μg/ml), and incubated for 4 h. Cells were counted after removing the top layer and staining. Cells were exposed to concentration of morphine, and then with naloxone at the optimal concentration. The control wells were incubated with the medium alone and wells to which fibroblast growth factor (13.5 ng/0.5 ml) was added served as the active comparator. Migration effects were presented as the % increase in

the number of cells over control divided by the difference between the fibroblast growth factor well and control (*e.g.*, the percent of the maximum effect on migration resulting from this concentration of fibroblast derived growth factor). Each series of concentration response curves were run at least three times and data pooled.

Quantitative Real-time Polymerase Chain Reaction for Collagen Type I Alpha 2 in Mouse Embryonic Fibroblasts. The mRNA levels of collagen type I α-2 were determined *via* quantitative polymerase chain reaction following the treatment with vehicle, morphine (10 μM), DMT-DALDA (10 μM), and PZM21 (10 μM). After the experimental treatment total RNA was isolated from the cells using TRIzol Reagent (Invitrogen, USA) and 1 μg of total RNA was used for cDNA synthesis by using iScript cDNA Synthesis Kit (Bio-Rad Laboratories, USA) according to the manufacturer's instructions. cDNA was amplified using real-time polymerase chain reaction in an ABI 7300 real-time polymerase chain reaction system (Applied Biosystems, USA). RNA analysis reagents (SYBR Green Master Mix) were from Bio-Rad, USA. We used the comparative ΔΔ cycle threshold method to quantify collagen type I α-2 gene expression. Target gene expression levels in the test samples were normalized to the endogenous reference glyceraldehyde-3-phosphate dehydrogenase (F: 5′-CCA ACC GCG AGA AGA TGA CC-3′ and R: 5′-GAT CTT CAT GAG GTA GTC AGT-3′) levels and reported as the fold difference relative to glyceraldehyde-3-phosphate dehydrogenase gene expression in the untreated baseline control. All assays were performed in triplicate and the experiments were repeated at least three times.

PRESTO-Tango Assay Screening for Mas-related G protein-coupled Receptor Activation. Human embryonic kidney T cells stably expressing a β-arrestin-TEV fusion protein and a tTa-dependent luciferase reporter were maintained in Dulbecco's Modified Eagle Medium (Corning, USA) containing 10% fetal bovine serum, 2 μg/ml puromycin, and 100 μg/ml hygromycin B at 37°C with 5% CO_2. Cells were plated to 50% confluency and transfected with a codon-optimized Mas-related G protein-coupled receptor-X Tango construct.[27] Transfected cells were transferred to glass-bottomed, poly-L-lysine-coated white 384-well plates (20,000 cells per well), and then were incubated for 18 to 24 h with concentrations of test article (in quadruplicate) diluted in drug buffer (1X Hank's Balanced Salt Solution with 20 mM [4-(2-hydroxyethyl)-1-piperazineethanesulfonic acid] and 0.3% bovine serum albumin, pH 7.4). After incubation, medium was removed and 20 μl of Bright Glo (a luciferase assay; Promega, USA; diluted 20-fold) was added and incubated 15 min at room temperature. Luminescence was measured on a TriLux luminescence counter and analyzed as relative luminescent units using GraphPad Prism (GraphPad Software, Inc., USA). Additional details are provided elsewhere.[28]

Statistics

Group Size. In the *in vivo* studies, no statistical power calculation to determine group size was conducted before the study. Group sizes were, however, projected to be a minimum of six guinea pigs per group, based on our previous work, showing that in the guinea pig model, the intrathecal concentrations of morphine employed in the current study produces increases in thermal escape latencies judged to be behaviorally relevant (6 to 8 s increases over baseline) and the ability to show significant increases in the incidence of intrathecal masses were statistically significant at the $P < 0.01$ (*post hoc* comparison with vehicle).[8]

Data Analysis. Data were compiled in Excel (v.14.4.9, Microsoft Corporation, USA), and statistical analyses were performed using Prism (v.6.0).

Statistical analysis protocols for each data set were based on the results of testing the null hypothesis of normality (Kolmogorov–Smirnov test) and homogeneity of Bartlett test). Graphics of data sets for which the null hypotheses were not rejected present the data as means ± SD and employed parametric statistics (one-way or two-way repeated measures ANOVA analysis with *post hoc* comparisons being made using the Dunnett test). A summary of these assessments of normality and homogeneity of variance is presented in the table in Supplemental Digital Content (http://links.lww.com/ALN/B941). Data sets that were considered nonparametric (histology scoring) or for which treatment groups showed rejection of the normality hypothesis were analyzed using a one-way analysis using a nonparametric statistic (Kruskal–Wallace) and a *post hoc* comparison performed using a Dunn test. Differences in the *post hoc* analyses reaching a $P < 0.05$ of significance were considered to be significant.

Results

Animal

A total of 71 guinea pigs were surgically prepared; 4 animals displayed motor dysfunction and did not recover and the catheter of one animal was lost after the start of infusion. These animals were euthanized and not included in subsequent analyses. A total of 66 animals were entered into and completed the studies. At necropsy, bolus injection of dye (10 μl: 0.5% weight by volume methylene blue) at study termination revealed uniformly intact catheters located within the intrathecal space at the level of the lumbar enlargement (approximately 11 cm from the cisterna magna).

Statistical Analyses

Failure to reject the null hypothesis regarding normality for each treatment data set (Kolmogorov–Smirnov test) and homogeneity of variances (Bartlett test) for each set of treatments with the thermal escape latency/area under curve

and mast cell degranulation data supported utilization of an ANOVA analysis. For the LAD2 studies, though groups sizes were too small to perform the Kolmogorov–Smirnov test, failure to reject the null hypothesis for homogeneity of variance and the observed covariance between means and medians led to use of ANOVA. For the fibroblast studies, where several treatment groups showed rejection of the normality hypothesis (see Supplemental Digital Content, table 1, http://links.lww.com/ALN/B941), we chose to employ a one-way repeated measures analysis using a nonparametric statistic.

Behavior

Intrathecal Morphine, DMT-DALDA, and PZM21 Infusions Yielded Comparable Antinociception. The intrathecal infusion at 0.5 μl/h of saline (fig. 1A) had no effect, but morphine (33 nmol · 0.5 μl^{-1} · h^{-1} = 12.5 μg · 0.5 μl^{-1}· h^{-1}; fig. 1B), DMT-DALDA (10 pmol · 0.5 μl^{-1} · h^{-1} = 9.8 pg · 0.5 μl^{-1} · h^{-1}), the potent μ agonist (fig. 1C), and PZM21 (28 nmol · 0.5 μl^{-1} · h^{-1} = 10.1 μg · 0.5 μl^{-1} · h^{-1}, the biased μ ligand; fig. 1D) all resulted in a significant near maximal increase in the thermal escape latency by day 3. This increase displayed a loss of effect such that by day 7, there was an evident reduction in the peak thermal escape latency for all three agonists. Analysis of effects produced by continuous infusion was accomplished by comparing the area under the curve for each drug (fig. 1E). This analysis showed a significant main effect with the *post hoc* analysis revealing that all were statistically greater than intrathecal saline, but not different from each other.

To specifically determine the effects of opioid antagonism on the formation of the intrathecal mass, guinea pigs receiving intrathecal infusion of morphine were prepared to receive the concurrent continuous subcutaneous infusion of saline or naltrexone (25 μg/h; Supplemental Digital Content, fig. S1 and table S2, http://links.lww.com/ALN/B942). Animals receiving intrathecal morphine (33 nmol/h) plus subcutaneous saline for 14 days displayed a significant antinociception on days 3 and 7 (comparable to that observed in fig. 1, B and E) as compared to their respective baselines (day 0). With the exception of day 1, where a modest and transient, but statistically significant increase was noted, animals receiving subcutaneous naltrexone displayed a complete block of the analgesic action of the concurrently delivered morphine (Supplemental Digital Content, figure S1, A and B, http://links.lww.com/ALN/B942).

Intrathecal Morphine, DMT-DALDA, and PZM21 Infusions Yielded Minimal Adverse Events. During the 14 to 16 days of infusion of saline, morphine, DMT-DALDA, or PZM21 at the indicated doses in animals shown in figure 1 and Supplemental Digital Content, figure S1 (http://links.lww.com/ALN/B942), there were no effects on pinnae or corneal reflexes. Motor functions (as defined by righting response, symmetrical ambulation, and hind paw proprioceptive function) were not altered in any animal at any time after the initiation of infusion, with the exception of one animal receiving intrathecal morphine on day 3 and one animal on day 1 receiving intrathecal DMT-DALDA, where mild hind limb motor weakness was noted. The only notable adverse events were the appearance of scratching and skin lesions in three animals receiving intrathecal morphine and a similar number in the group receiving intrathecal morphine and subcutaneous naltrexone. Scratching was largely absent after day 7 and skin lesions resolved. No such events were noted with DMT-DALDA or PZM21.

Spinal Mass Formation

Morphine, but Not DMT-DALDA or PZM21, Induces Prominent Intrathecal Masses. In the current work, we systematically assessed the histopathology of the spinal intrathecal space in catheterized guinea pigs after the 14 days of infusion of saline, morphine, DMT- DALDA or PZM21. In this work, the primary finding was the appearance of a space-occupying mass proximal to the lumbar catheter tip. These masses were graded on a 0 to 4 scale, as shown in the representative sections presented in figure 2, and separately by a forced ranking of the mass by size and degree of cord compression. Observer ranking concordance calculated as previously described[10] showed that the intraclass correlation was found to be acceptable (intraclass correlation = 0.931), with an F value greater than 0.1, indicating no difference between raters, and a high level of concordance for the pathology grading. This analysis of the intrathecal mass by treatment group is presented in figure 3, A and B, respectively. As indicated, while the three opioids examined were delivered in approximately equianalgesic concentrations (fig. 1), only the intrathecal infusion of morphine resulted in prominent intrathecal masses. The median and interquartile range of the pathology grade for morphine (2.3: 2.0 to 3.5) were greater as compared to DMT-DALDA (1.0: 0.6 to 1.4), PZM21 (0.5: 0.5 to 1.8), and saline (1.3: 1.0 to 1.5).

Subcutaneous Naltrexone Infusion Blocks Analgesia but Not Mass Formation by Intrathecal Morphine. An important question was whether the mass-producing effect of morphine was reversed by an ongoing opioid receptor antagonist. The continuous subcutaneous delivery of naltrexone, a pan opioid receptor antagonist, completely reversed the analgesic effects of intrathecal morphine (Supplemental Digital Content, figure S1, A and B, http://links.lww.com/ALN/B942), but on the contrary had no effect upon the intrathecal mass score or rank (fig. 3, A and B).

Intrathecal Masses Constituted of Local Collections of Fibroblasts and Collagen. Histopathology emphasized several common observations. (1) As previously reported, the intrathecal mass in the guinea pig was localized to no more than 2 to 3 segments rostrally and caudally to the catheter tip, and was typically of sufficient girth as to yield varying degrees of local compression of the spinal cord. (2) Figure 4

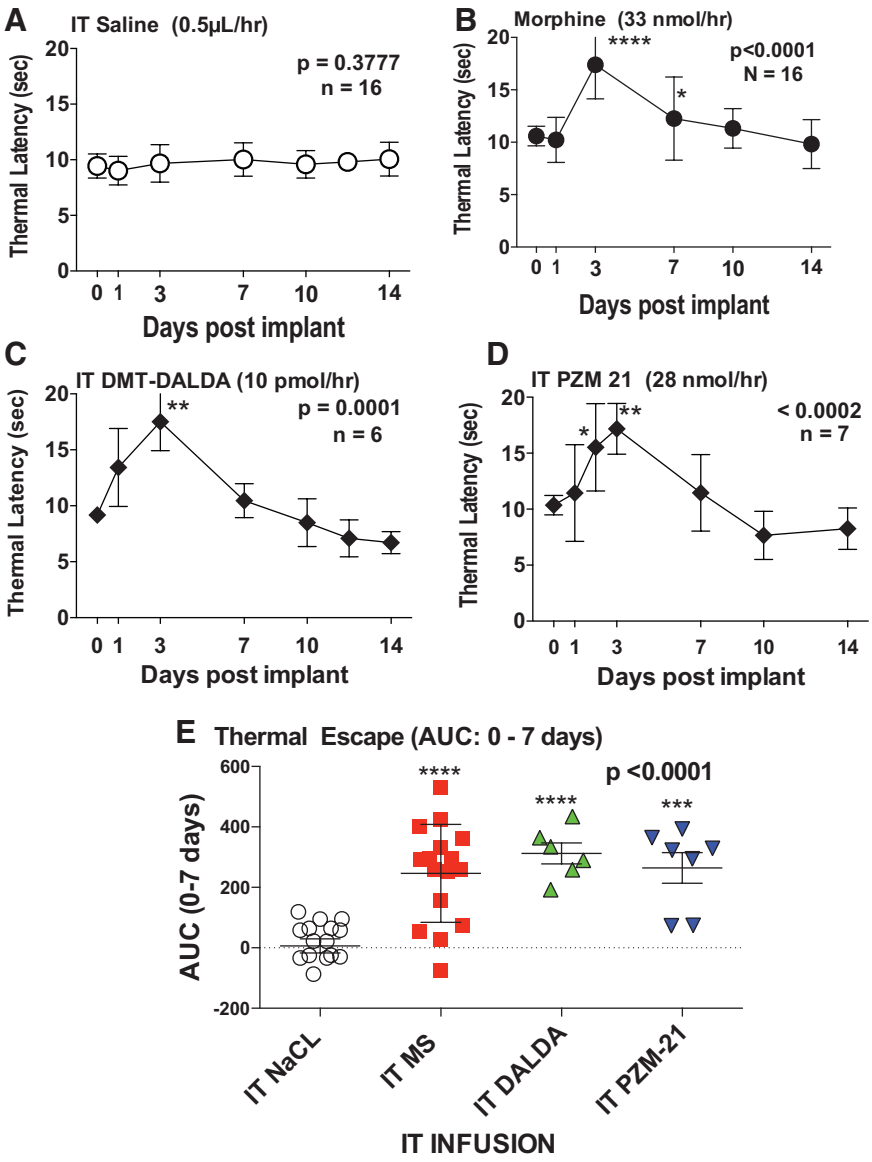

Fig. 1. Time course depicting the mean ± SD of the hind paw thermal escape latency (s) *versus* time in rats prepared with chronic intrathecal (IT) catheters connected to osmotic pumps delivering 0.5 µl/h for 14 days and loaded to deliver: (*A*) saline (vehicle, 0.5 µl/hr); (*B*) morphine (33 nmol/h); (*C*) DMT-DALDA (10 pmol/h) or (*D*) PZM21 (28 nmol/h). (*E*) Area under the curve (AUC) (mean ± SD) was calculated from baseline to day 7 for the four treatment groups. For the time course curves, one-way repeated measures ANOVA were performed with Dunnett multiple comparison tests *versus* day 0 (immediately before implantation). For the AUC data, analysis was by a one-way nonrepeated ANOVA with a Dunnett multiple comparison tests *versus* saline infusion: **P* < 0.05; ***P* < 0.01; ****P* < 0.001; *****P* < 0.0001. MS, morphine sulfate; NaCl, sodium chloride.

demonstrates tissue from a guinea pig receiving intrathecal morphine showing the mass. Though closely adherent to the pial surface, it could be observed to be structurally distinct from the cord parenchyma with the demarcation being the pia (fig. 4C). Collagen staining tendrils could occasionally be observed to penetrate the pial layer. (3) In contrast, the mass was closely integrated with the adjacent dura-arachnoid. In this single section (fig. 4, B and D), the orientation and distribution of the fibroblasts can be seen apparently migrating from the dura into the intrathecal mass along with collagen-positive fibers. (4) The mass typically showed little inflammatory infiltrate and, based on the histopathology, was largely constituted of fibroblasts in a dense developing collagen matrix (fig. 4, B and C). (5) Herovici staining for collagen was predominately blue (emphasizing young, newly deposited collagen), with faint red staining (mature) in the outer regions of the mass, consistent with a mass growing from the inside (adjacent

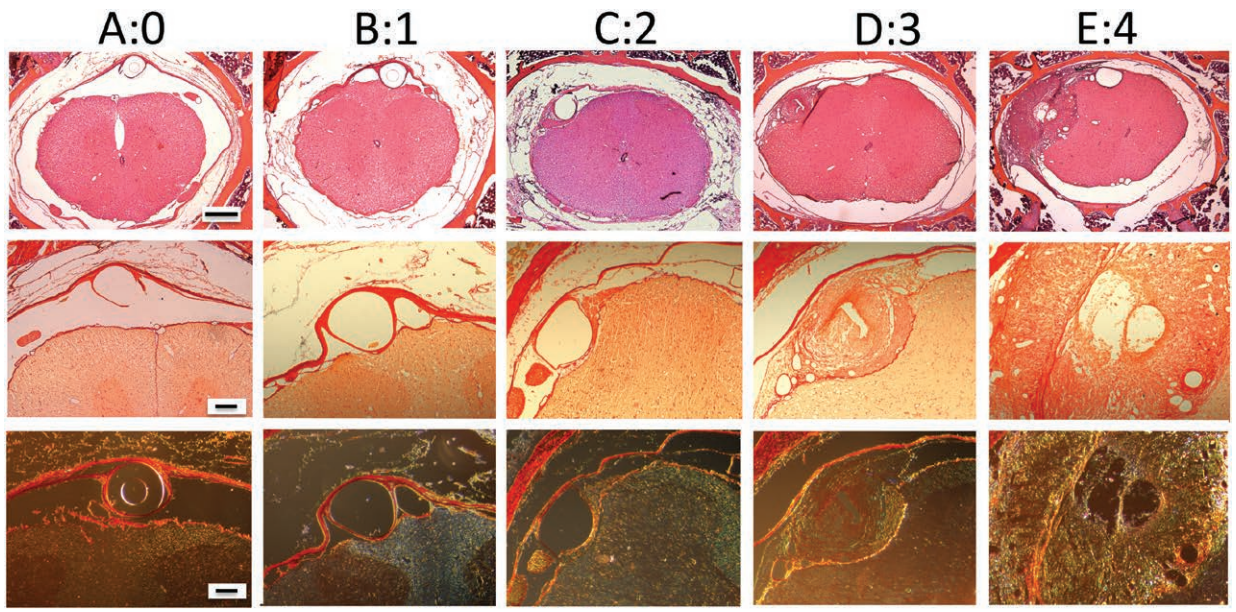

Fig. 2. Representative histopathology of decalcified lumbar vertebral blocks collected proximal to the lumbar catheter tip from guinea pigs receiving 14-day intrathecal infusions showing representative pathology which was graded as: 0 (*A*); 1 (*B*); 2 (*C*); 3 (*D*): and 4 (*E*). The top row represents low magnification of hematoxylin and eosin–stained decalcified spinal blocks (size bar = 500 μm). The middle and bottom rows are an adjacent section imaged at a higher magnification (size bar = 100 μm) stained with Picro-Sirius and imaged (middle row) with normal light (*red* indicating collagen) and with polarized light (bottom row) indicating type 1 collagen (*yellow-orange* birefringence and type II collagen with *green* birefringence. As indicated, grades of 2 or greater are considered to represent meaningful histologically defined spinal masses. MS, morphine sulfate.

to the catheter and morphine infusate) (fig. 4E through G). Again, the Herovici stain emphasizes the demarcation of the mass at the pia (fig. 4F) and the collagen tendrils entering the mass from the dura-arachnoid (fig. 4G). (6) Using Picro-Sirius under bright field, dense collagen staining could be observed (fig. 4, H and I). With polarized light, the birefringence imaging revealed thick (yellow-orange birefringence) and to a lesser degree, thin (green birefringence) collagen fibers, indicative of types 1 and 3 collagen, respectively, could be readily observed (fig. 4J). As we have previously noted, the cellular composition of the mass in hematoxylin and eosin sections consisted of sparse macrophages and few lymphocytes.[8,9]

Mast Cell Degranulation

Morphine but Not PZM21 or DMT-DALDA Evokes Mast Cell Degranulation In Vitro. Our previous work with the morphine-evoked intrathecal mass emphasized the likely role of meningeal mast cells. In the current study, the absence of an effect upon mass formation of equianalgesic intrathecal infusion doses of DMT-DALDA and PZM21 raised the question of whether these agents could degranulate mast cells. Using the LAD2 human mast cell line, we confirmed that morphine indeed was a potent mast cell degranulator (fig. 5). In previous work we have shown in several models that the degranulating effects of morphine were not naloxone antagonized, but were prevented by the mast cell stabilizer, cromolyn.[12] In contrast to morphine, PZM21 had no effect upon mast cell degranulation. DMT-DALDA resulted in a significant degranulation as compared to control, but only at the highest concentration (10 μM) examined.

Fibroblast Activation

Morphine but Not PZM21 or DMT-DALDA Enhances Proliferation of Fibroblasts In Vitro. To determine if morphine promotes mouse embryonic fibroblast proliferation, mouse embryonic fibroblasts were incubated with morphine at doses ranging from 0.3 nM to 300 μM. Morphine at 3 and 30 μM significantly enhanced fibroblast proliferation as compared to the control. A peak affect was observed at 3 μM (fig. 6A). Additional studies were carried out with the potent μ-opioid agonist (fentanyl; fig. 6B), the biased μ-opioid agonist PZM21 (fig. 6C), the potent μ-opioid agonist DMT-DALDA (fig. 6D). Though employed in a similar range of concentrations as used with morphine, these agents had no effect upon fibroblast proliferation.

Morphine Fibroblast Proliferative Effects Were Unaffected by Naloxone, but Prevented by Cromolyn. To determine whether the proliferative effects of morphine were opioid receptor–mediated, fibroblasts were treated with a combination of morphine and naloxone in equimolar concentrations.

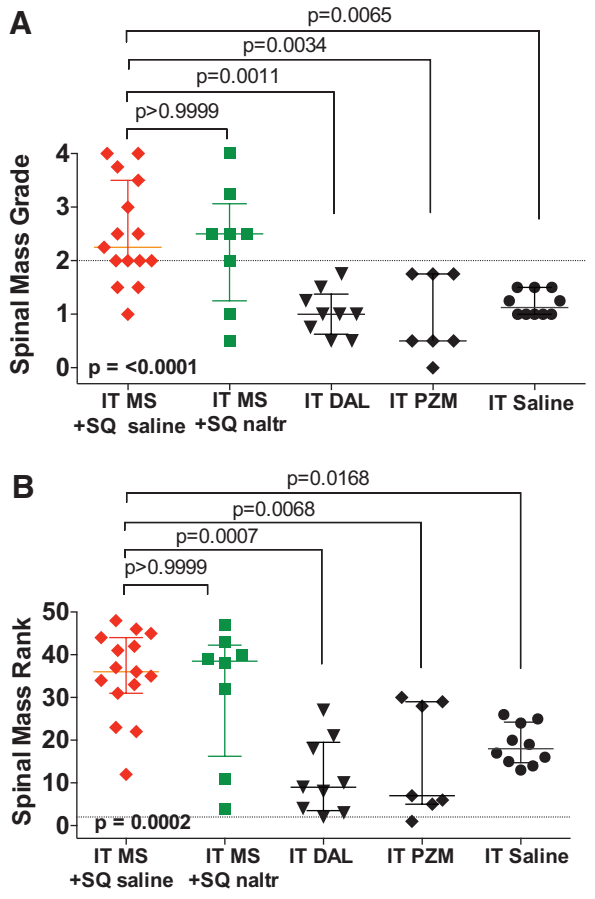

Fig. 3. Scattergrams displaying medians with quartiles for: (*A*) grading of intrathecal mass (0 to 4), and (*B*) rank ordering from least (rank 1) to greatest severity of intrathecal (IT) mass. For analysis, IT morphine + subcutaneous (SQ) saline was merged with IT morphine alone and IT saline + SQ naltrexone was merged with IT saline. The IT mass score for IT morphine with and without naltrexone were not different from each other but were significantly greater than that for IT saline. Mass scores for IT DMT-DALDA and IT PZM21, like saline, were significantly less than those for IT morphine. Similar results were observed with the blind ordering of the ranking of the masses (from least to greatest). Group comparisons employed a Kruskal–Wallace nonparametric one-way ANOVA and Dunn *post hoc* comparison. Exact *P* values are presented.

As shown, naloxone did not inhibit morphine-induced proliferation of fibroblasts (fig. 6E). As cromolyn attenuated mast cell degranulation and prevented mass formation in the canine model,[11] we also examined the effects of cromolyn on the promotion by morphine of fibroblast proliferation. Here we found that cromolyn indeed reversed the proliferation otherwise produced by morphine in the absence of mast cells (fig. 6F).

Morphine Enhances the Migration of Fibroblasts In Vitro. Morphine induced significant mouse embryonic fibroblast migration at doses 2 to 20 μM, respectively. Naloxone at equimolar and up to 10× the equimolar concentrations of morphine (20 μM) did not prevent migration induced by morphine (Supplemental Digital Content, figure S2 (http://links.lww.com/ALN/B943).

Morphine but Not PZM21 or DMT-DALDA Enhances Fibroblast Collagen mRNA Expression. Treatment of mouse embryonic fibroblasts with morphine (10 μM) within the concentration range producing fibroblast proliferation resulted in a significant increase in collagen type I α-2 mRNA as measured by quantitative polymerase chain reaction. In contrast, treatment with equimolar concentrations of DMT-DALDA (10 μM) or PZM21 (10 μM) had no effect as compared to buffer control (fig. 7).

PRESTO-Tango Assay Screening for Mas-related G protein-coupled Receptor-X Activation

Morphine but Not PZM21 or DMT-DALDA Activates Mas-related G Protein-coupled Receptor-X. Current work has shown that an important cascade for degranulating mast cells is through the activation of Mas-related G protein-coupled receptor-X2. Using the PRESTO-Tango assay, we assessed the effects of these several opioid ligands on their ability to activate Mas-related genes. As shown in figure 8, Tan 67 (a δ-opioid agonist), morphine and DMT-DALDA all resulted in near maximal degrees of activation with the Log EC50 (M) being −5.8, −5.1, and −4.7, respectively. In contrast, as fentanyl and the biased μ ligands PZM21 and TRV130 failed to produce a saturating curve, the EC50s could not be calculated and the compounds can be said only to show some activity in the PRESTO-Tango assay at approximately 100 μM. These results with morphine, DMT-DALDA, and PZM21 are consistent with the relative effects of these agents on mast cell degranulation (fig. 5) and fibroblast activation (fig. 6 and 7). Given the ability of cromolyn to prevent mast cell degranulation and fibroblast activation, separate studies were undertaken to determine if cromolyn activated Mas-related genes in the PRESTO-Tango assay. It did not. Further, coincubation of cromolyn with morphine or a full agonist (mitiglinide) or a partial agonist at the Mas-related G protein-coupled receptor-X receptor did not alter their evoked Mas-related gene activation (Supplemental Digital Content, figure S3, http://links.lww.com/ALN/B944). These results indicate that cromolyn is neither an agonist nor an antagonist at the Mas-related G protein-coupled receptor-X receptor, as measured by the Tango arrestin recruitment assay.

Discussion

Intrathecal opiate use is impacted by the risk of producing space-occupying intrathecal masses. The present work provides specific insights into mechanisms whereby opiate

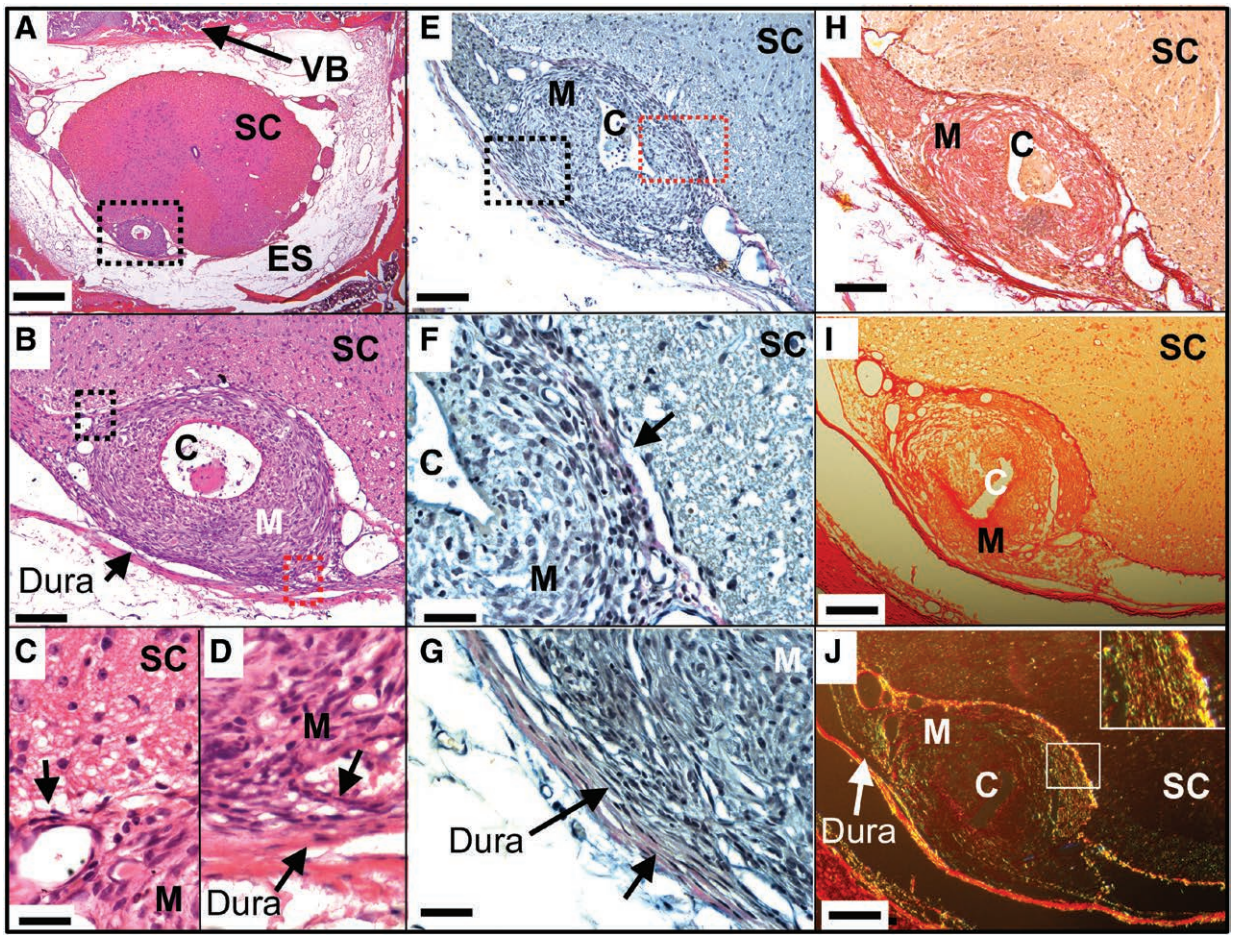

Fig. 4. Representative spinal histopathology of a guinea pig which received 14-day intrathecal infusion of morphine (33 nmol/h). (*A*) Brightfield section stained with hematoxylin and eosin and imaged at (*A*) 4×, (*B*) 20×, and (*C/D*) 60×, where size bars are 500 μm, 100 μm, and 30 μm, respectively. The *dotted box* in *A* is the area imaged in *B*, and the *dotted black* (left) and *red boxes* (right) in *B* are the areas imaged in *C* and *D*, respectively. In *C*, one sees the clean demarcation of mass and spinal cord at the pial/parenchymal boundary (*short black arrow*), whereas in *D*, one sees tendrils of collagen arising from the adjacent dura connecting to the adjacent mass (*short black arrow*). (*E*) An adjacent section is stained with Herovici for collagen and imaged at 20×. *Black* and *red dotted boxes* indicate areas for *F* and *G*, respectively (60×), where size bars are 100 μm and 30 μm, respectively. The *short black arrows* in *F* and *G* point to the red hue that represents mature collagen at the margins of the spinal mass and in the dura. (*F*) One can see the clear interface between the fibroblast-rich mass and the spinal parenchyma. (*G*) One sees the tendrils of collagen arising from the adjacent dura. (*H*) Bright field hemaoxylin and eosin with adjacent section showing mass and parenchyma (*I*) section stained with Picro-Sirius for collagen and imaged with brightfield at 20× or in polarized light (*J*) to observe birefringence. (*H*) *Orange* represents collagen, while in *I* the *yellow-orange* birefringence represents type 1 (thick) fibers and *green* birefringence represents type 3 (thin) collagen. Inset in *J* is 60× showing *green* and *yellow* birefringence. C, catheter; Dura, dura-arachnoid; ES, epidural space; M, Mass; SC, spinal cord; VB, vertebral body.

agonists initiate intrathecal masses by signaling through the noncanonical Mas-related gene pathway.

Analgesia

The first issue is that the agents examined at the respective doses resulted in an equianalgesic activity. Morphine, PZM21, a biased μ ligand, or DMT-DALDA, a dermorphin-derived μ-opioid peptide, were delivered by intrathecal infusion in concentrations producing a comparable increase in escape latencies. The molar potency ratio of these molecules in the infusion paradigm was approximately 1: 0.8: 3000. All agents resulted in analgesia by days 2 to 3 and all showed loss of effect by day 7. This timeframe is observed in the rat and guinea pig.[29,30] While the role of mass formation in loss of analgesia for morphine was not assessed, this loss of effect was observed with PZM21 and DMT-DALDA, which did not produce a mass. Although some suggest that biased ligands may show differences in development of tolerance,[31–33] this was not observed after intrathecal (current studies) or systemic delivery.[34] At these doses, minimal adverse effects were observed

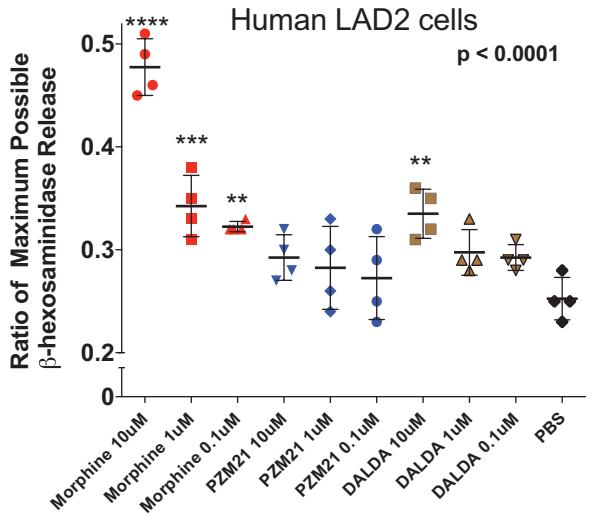

Fig. 5. Graph presents the scatter plot of mast cell degranulation as measured by the concentrations of ß-hexosaminidases in the supernatant of human LAD2 cells incubated with increasing concentrations (0.1 to 10 μM) of morphine, PZM-2,1 and DMT-DALDA. Y-axis plots the release of β-hexosaminidase presented as the ratio of the maximum possible release produced by compound 48 to 80. Each point represents a single well. Data were analyzed with a one-way ANOVA followed by a *post hoc* comparison to phosphate-buffered saline (PBS). $^{**}P < 0.01$; $^{***}P < 0.001$; $^{****}P < 0.0001$.

with either PZM21 or DMT-DALDA. Morphine was characterized by an incidence of caudally directed scratching and skin lesions during the first 7 to 10 days, which resolved.

Intrathecal Mass

Intrathecal masses arise from the dura-arachnoid proximal to the site of intrathecal delivery (fig. 4).[6,9] While referred to as an "inflammatory" mass, it is largely composed of fibroblasts in a dense collagen matrix.[8,9] Intrathecal fibrosis is observed after a variety of pathologies (*e.g.*, subarachnoid hemorrhage) which, in humans, as in the intrathecal mass observed in guinea pig and dog, is composed of collagen types 1 and 3.[8,35,36] The mass presents as a progressive expansion from the catheter outwards with less mature (newly created) collagen observed proximal to the catheter and mature collagen present in the outer margins.[8] Sequential magnetic resonance imaging in dogs receiving morphine infusion revealed a time-dependent enlargement of the mass.[6,37] In early stages, substitution of saline results in a reduction in mass size. Termination in the late phase reveals a mature mass that resolves slowly, consistent with the mature collagen outlining the masses in guinea pig and dog.[8]

Pharmacology of the Intrathecal Mass

While a catheter can initiate a reaction,[8] the enlarging mass is not a simple response to catheter or infusion,[6,38] infection,[6,39] or formulation.[1] Preclinical studies show that intrathecal masses are produced by several (morphine, hydromorphone, methadone), but not all (fentanyl, alfentanil) opioids,[6,10,11] a profile largely recapitulated in humans.[40,41] Further, μ-opioids DMT-DALDA[18,19] and PZM21[42] resulted in analgesia but failed to produce an intrathecal mass. This profile is consistent with failure of opioid antagonism to block formation of masses in dogs[1] and, as shown here, in guinea pigs.

Role of the Meningeal Mast Cell

In primary mast cell cultures and in the wheal-flare response after subcutaneous delivery in dog, three observations were made. (1) Agents that degranulate mast cells (morphine, hydromorphone, and methadone) result in an intrathecal mass, while those that do not degranulate (fentanyl or alfentanil) have not been reliably associated with spinal masses.[10–12] (2) Degranulating effects of morphine were not blocked by naloxone[12] and neither were the effects of intrathecal morphine in producing masses (current studies).[9] (3) Further, in dogs, cromolyn sodium (mast cell stabilizer) diminished degranulation/fibroblast activation and attenuated development of morphine-induced spinal masses.[9] In the current work, we confirmed this association by showing that PZM21 failed to produce degranulation/activation or a mass while DMT-DALDA did so in concentrations comparable to those of morphine, but the equianalgesic intrathecal concentration for DMT-DALDA was in the pmol/h *versus* nmol/h range.

Mas-related Gene Signaling

Mas-related G protein-coupled receptors are classified as orphan G protein-coupled receptors and implicated in IgE-independent inflammatory responses in mast cells.[14,43] Morphine-evoked increases in intracellular calcium and mast cell degranulation occur through Mas-related G protein-coupled receptor signaling.[15] Using the PRESTO-Tango assay, morphine and DMT-DALDA resulted in activation of Mas-related G protein-coupled receptor-X2. In contrast, PZM21 and fentanyl produced a degree of activation only at 100 μM. While saturating concentrations for these drugs in this assay was not examined, these results correspond to the modest effect of these agents on mast cell degranulation/fibroblast activation where, in contrast, morphine yielded the greatest effects. DMT-DALDA, a μ-opioid peptide, was only modestly active and then only so at the highest concentration. PZM21 had no effect on mast cell degranulation. Though not studied here, our previous work with fentanyl in human mast cell cultures and dog skin after intradermal injection displayed, in contrast to morphine and hydromorphone, little or no effect on mast cell degranulation.[12]

Intrathecal infusion at equianalgesic concentrations of morphine, but neither PZM21 nor DMT-DALDA, yielded an intrathecal mass. The lack of effect of PZM21 corresponds with its lack of effect on Mas-related G protein-coupled

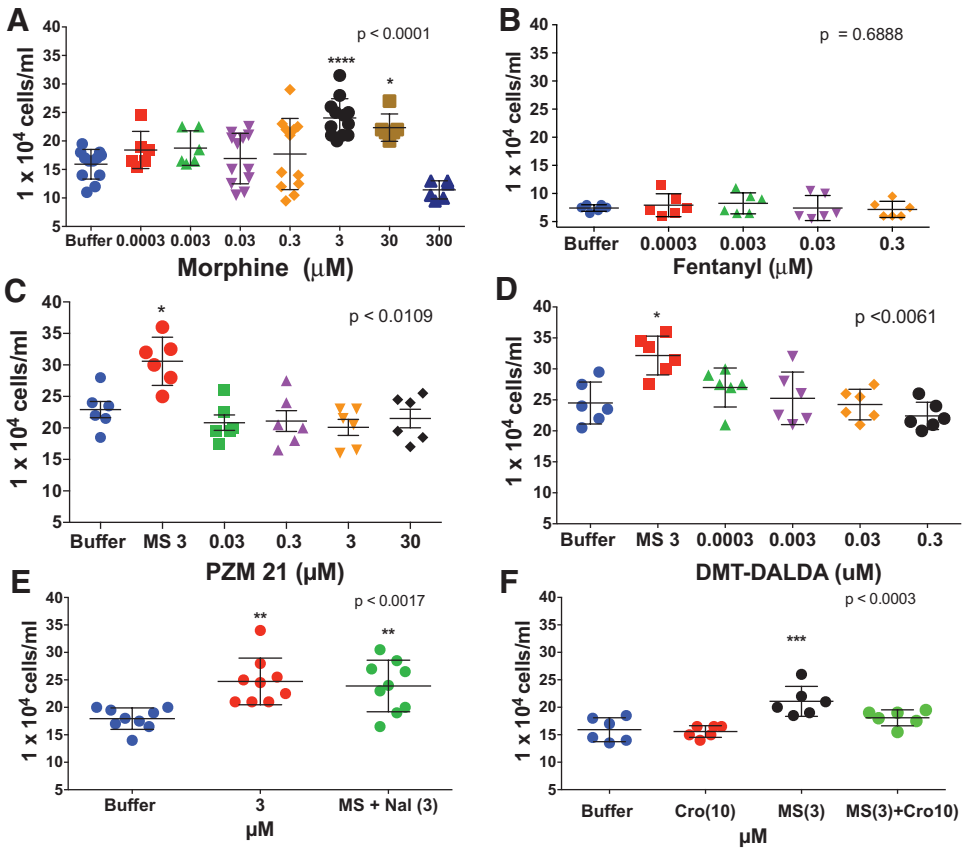

Fig. 6. Scattergrams display the proliferative response of mouse embryonic fibroblasts (MEFs) after 48 h in the presence of: (*A*) vehicle or 0.3 nM to 300 μM morphine, with the maximum proliferative response produced by 3 μM; (*B*) vehicle or morphine (MS: 3 μM) or morphine (3 μM) + naloxone (Nal: 3 μM) showing that the proliferative effects of morphine were not altered by equimolar concentrations of the opioid antagonist; (*C*) vehicle or morphine (3 μM) or PZM21 (0.03 to 30 μM) showing no effect of PZM21; (*D*) vehicle or morphine (3 μM) or DMT-DALDA (0.03 to 30 μM) showing no effect of DMT-DALDA; and (*E*) 0.3 pM to 300 nM fentanyl for 48 h. (*F*) Vehicle or morphine (MS: 3 μM) or 48 to 80 (1 μg/ml) or morphine (3 μM)/ 48 to 80 (1μg/ml) + cromolyn (Cro: 10 μM) showing that the proliferative effects of morphine were mimicked by 48 to 80 and prevented by the mast cell stabilizer. Each point represents a single well. For each drug, a one-way ANOVA was performed and a *post hoc* analysis was performed comparing vehicle. $P < 0.05$; $^{**}P < 0.01$; $^{***}P < 0.001$. MS, morphine sulfate.

receptors and on its failure to yield mast cell degranulation and fibroblast activation. While DMT-DALDA yielded measurable degranulation and activation at concentrations comparable to those employed by morphine, the DMT-DALDA concentration required was 0.001× that required for morphine. Accordingly, failure to see a mass with DMT-DALDA indicates that concentrations necessary to produce analgesia were substantially less than those concentrations required to produce meningeal mast cell degranulation. A similar circumstance holds for the Cav 2.2 channel blocker, ziconotide, which is a potent mast cell degranulator,[12] but is not considered to be associated with mass formation. This reflects the low intrathecal ziconotide concentrations required for analgesia *versus* concentrations required to produce mast cell degranulation.[12] Based on the above, we predict that TRV130 (oliceridine), a biased μ ligand that did not activate Mas-related genes and did not degranulate mast cells or activate fibroblasts, would not result in a mass. In contrast, TAN67 (a δ-opioid agonist) would yield all three effects, if, unlike DMT-DALDA, it required a high dose to produce analgesia.

Fibroblasts

The intrathecal mass is a fibroblast-rich collagen matrix arising from the meninges. In fibroblast cultures, absent mast cells, morphine, in a naloxone-insensitive fashion, but not PZM21 or DMT-DALDA in concentrations comparable to those studied in the degranulation of mast cells, resulted in fibroblast proliferation in cell culture which was prevented by cromolyn. Quantitative polymerase chain reaction for collagen type I revealed that morphine, but not DMT-DALDA or PZM21, increased collagen type

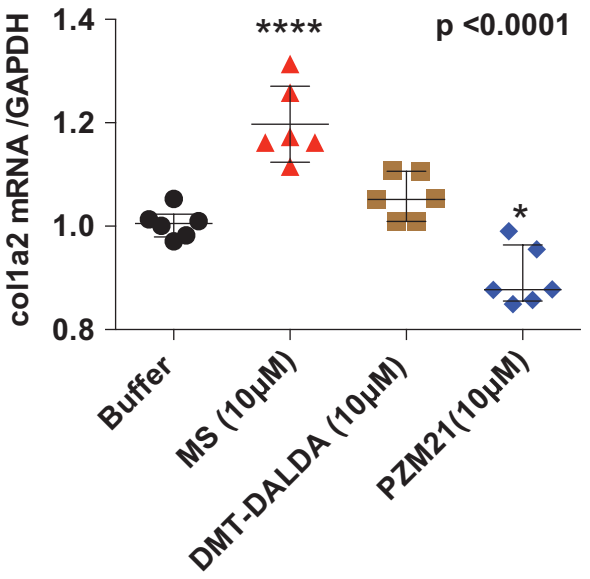

Fig. 7. Scattergrams display the levels (mean ± SD) of collagen type I α2 mRNA as a ratio to Glyceraldehyde 3-phosphate dehydrogenase (GADPH) as measured by quantitative polymerase chain reaction of samples coincubated with morphine (MS: 10 μM), DMT-DALDA (DALDA: 10 μM), or PZM21 (10 μM), or buffer control. Each point represents a single well. One-way ANOVA was performed and a *post hoc* analysis was performed. Treatments linked by a common line did not differ. ***$P < 0.001$.

1 mRNA, suggesting that fibroblast activation may also be accomplished in an Mas-related gene–dependent fashion. Microarray data bases indeed report that human cutaneous fibroblasts involved in keloid scar formation express the Mas-related gene family, with the rank ordering of expression being Mas-related genes 2 and 4 greater than 1 and 3.[44]

Activation of Mast Cells and Fibroblasts as a Mechanism of Mass Formation. Our hypothesis associating Mas-related gene signaling in mast cells and fibroblasts and mass formation hinges on four observations derived from cultured mast cells and fibroblasts and *in vivo* spinal infusions: (1) an opiate that activates Mas-related genes, degranulates mast cells and activates fibroblasts produces a spinal mass (morphine); (2) an opiate that does not activate Mas-related genes, does not degranulate mast cells, or activate fibroblasts does not produce a spinal mass (PZM21); (3) an opiate which activates Mas-related genes, degranulates mast cells, and activates fibroblasts, but is significantly more potent as a μ agonist does not produce masses at equianalgesic concentrations to morphine; and (4) a mast cell stabilizer (cromolyn) blocks morphine induced mast cell degranulation, fibroblast activation, and as previously reported, reduces mass formation. The cellular mechanism of cromolyn is not well defined.[45] We exclude a direct interaction with Mas-related genes. The present work suggest that the fibroblast rich mass results from at least two nonexclusive processes.

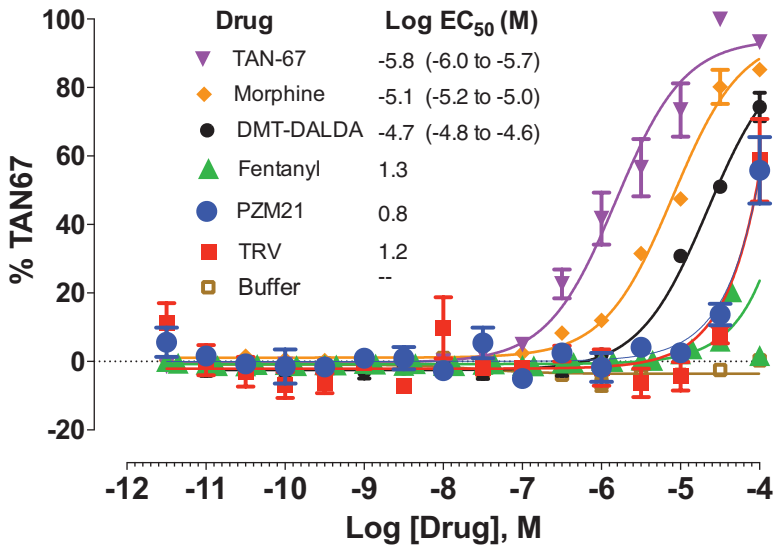

Fig. 8. Graph presents the concentration response curves for the PRESTO-Tango assay showing Mas-related gene activation by TAN-67, morphine, DMT-DALDA, PZM21, TRV-130 (TRV), fentanyl, and buffer. Y-axis expresses the activation in terms of the percentage of the response observed with TAN-67. Best fit log regression curves are presented. The inserted table presents the calculated Log EC_{50}, with 95% CI for each of the test compounds. PRESTO-TANGO, Parallel Receptor-ome Expression and Screening *via* Transcriptional Output; TRV, transient receptor potential cation channel.

(1) *Indirect pathway to fibroblast activation*. Degranulation of meningeal mast cells through Mas-related gene engagement leads to release of tryptases and chymases, inducing fibroblast proliferation and migration,[13,46–48] while blocking degranulation reduces dermal fibroblast chemotaxis and inhibiting mast cell function decreases scar formation.[46,47,49,50]
(2) *Direct pathway to fibroblast activation*. Activation of Mas-related genes in meningeal fibroblasts lead to proliferation, migration and collagen secretion. This mechanistic profile closely resembles events underlying keloid scarring where exuberant fibroblast activation is enhanced by mast cell activation. Hence, we may consider the intrathecal mass to be a keloid scar of the meninges.
(3) *An additional pathway may also exist*. A spinal mass resected from a patient receiving 50 mg/ml displayed morphine particulates.[51] Intrathecal particulates (methylprednisolone acetate,[52] talcum powder, and starch[53]) can also initiate meningeal reactions.

Study Limitations

The direct effect of opioids on fibroblasts and mast cells are demonstrated in *in vitro* cell culture experiments. The linkage between *in vitro* studies showing activation and spinal masses (*in vivo*) is indirect, based on parallels between the Mas-related gene agonist pharmacology and inhibitory effects of cromolyn on mast cell and fibroblast activation and spinal mass formation by agents activating Mas-related genes.

Clinical Impact

Incidence of intradural masses with chronic opiate infusion is estimated to be around 8%.[40] The role of concentration presents a conundrum for intrathecal delivery given the need to provide sufficient activation with infusate volume constraints posed by implanted pumps. Agents that do not activate Mas-related genes (PZM21) or do so at concentrations above those required for analgesia (DMT-DALDA) may provide an alternate approach to activating potent regulatory control over spinal nociceptive processing.

Acknowledgments

The authors would like to thank Brian Shoichet, Ph.D., Department of Pharmaceutical Chemistry, University of California, San Francisco, California, and Bryan Roth, M.D., Ph.D., Department of Pharmacology, University of North Carolina, Chapel Hill, North Carolina, for their specific commentaries on the interpretation of the PRESTO-TANGO assay results and the properties of biased opiate receptor ligands, and Julio Medina, Ph.D., of Epiodyne, San Francisco, California, for providing the PZM21. The support for the Tango assays came from the National Institute of Mental Health Psychoactive Drug Screening Program (Bethesda, Maryland; Dr. Roth). The authors also thank Matt Hunt, B.S., M.S., University of California, San Diego, California, for his important input on Mas-related gene expression in fibroblasts. The authors would also like to express their recognition of the role played by Frederick W. L. Kerr, M.D. (1923 to 1983), Department of Neurosurgery, Mayo Clinic, Rochester, Minnesota, in advancing the therapeutic development of spinal opiates, Burton M. Onofrio, M.D., Department of Neurosurgery, Mayo Clinic, for his implementation of the first intrathecal pump, and Christopher M. Bernards, M.D. (1958 to 2012), Virginia Mason, Seattle, Washington, who suggested the importance of mast cells in the intrathecal mass.

Competing Interests

Early portions of the in-life guinea pig work examining naltrexone effects of the morphine mass was supported by funds from Medtronic (Minneapolis, Minnesota) provided to Dr. Yaksh. Dr. Hildebrand and Dr. Page are Medtronic employees and contributed to the design of the studies and preparation of the final manuscript. Dr. Griener holds a patent position on the discovery of PZM21. Dr. Schiller holds a patent position on the discovery of DMT-DALDA.

Research Support

This work was supported by National Institutes of Health grant No. R01 NIDA015353 (Bethesda, Maryland; to Dr. Yaksh) and funds from Medtronic (Minneapolis, Minnesota) supporting early portions of the *in vivo* guinea pig work.

Correspondence

Address correspondence to Dr. Yaksh: Department of Anesthesiology, University of California, San Diego, 9500 Gilman Dr., La Jolla, California 92093. tyaksh@ucsd.edu.

References

1. Yaksh TL, Fisher C, Hockman T, Wiese A: Current and Future Issues in the development of spinal agents for the management of pain. Curr Neuropharmacol 2016; 152: 232–59
2. Yaksh TL: Spinal opiate analgesia: Characteristics and principles of action. Pain 1981; 11:293–346
3. Onofrio BM, Yaksh TL, Arnold PG: Continuous low-dose intrathecal morphine administration in the treatment of chronic pain of malignant origin. Mayo Clin Proc 1981; 56:516–20
4. North RB, Cutchis PN, Epstein JA, Long DM: Spinal cord compression complicating subarachnoid infusion of morphine: Case report and laboratory experience. Neurosurgery 1991; 29:778–84

5. Yaksh TL, Hassenbusch S, Burchiel K, Hildebrand KR, Page LM, Coffey RJ: Inflammatory masses associated with intrathecal drug infusion: A review of preclinical evidence and human data. Pain Med 2002; 3:300–12
6. Yaksh TL, Horais KA, Tozier NA, Allen JW, Rathbun M, Rossi SS, Sommer C, Meschter C, Richter PJ, Hildebrand KR: Chronically infused intrathecal morphine in dogs. Anesthesiology 2003; 99:174–87
7. Gradert TL, Baze WB, Satterfield WC, Hildebrand KR, Johansen MJ, Hassenbusch SJ: Safety of chronic intrathecal morphine infusion in a sheep model. Anesthesiology 2003; 99:188–98
8. Eddinger KA, Rondon ES, Shubayev VI, Grafe MR, Scadeng M, Hildebrand KR, Page LM, Malkmus SA, Steinauer JJ, Yaksh TL: Intrathecal catheterization and drug delivery in guinea pigs: A small-animal model for morphine-evoked granuloma gormation. Anesthesiology 2016; 125:378–94
9. Yaksh TL, Allen JW, Veesart SL, Horais KA, Malkmus SA, Scadeng M, Steinauer JJ, Rossi SS: Role of meningeal mast cells in intrathecal morphine-evoked granuloma formation. Anesthesiology 2013; 118:664–78
10. Allen JW, Horais KA, Tozier NA, Yaksh TL: Opiate pharmacology of intrathecal granulomas. Anesthesiology 2006; 105:590–8
11. Yaksh TL, Steinauer JJ, Veesart SL, Malkmus SA: Alfentanil: correlations between absence of effect upon subcutaneous mast cells and absence of granuloma formation after intrathecal infusion in the dog. Neuromodulation 2013; 16:459–66; discussion 466
12. Schmidt-Rondon E, Wang Z, Malkmus SA, Di Nardo A, Hildebrand K, Page L, Yaksh TL: Effects of opioid and nonopioid analgesics on canine wheal formation and cultured human mast cell degranulation. Toxicol Appl Pharmacol 2018; 338:54–64
13. Singhal PC, Sharma P, Sanwal V, Prasad A, Kapasi A, Ranjan R, Franki N, Reddy K, Gibbons N: Morphine modulates proliferation of kidney fibroblasts. Kidney Int 1998; 53:350–7
14. Tatemoto K, Nozaki Y, Tsuda R, Konno S, Tomura K, Furuno M, Ogasawara H, Edamura K, Takagi H, Iwamura H, Noguchi M, Naito T: Immunoglobulin E-independent activation of mast cell is mediated by Mrg receptors. Biochem Biophys Res Commun 2006; 349:1322–8
15. Lansu K, Karpiak J, Liu J, Huang XP, McCorvy JD, Kroeze WK, Che T, Nagase H, Carroll FI, Jin J, Shoichet BK, Roth BL: In silico design of novel probes for the atypical opioid receptor MRGPRX2. Nat Chem Biol 2017; 13:529–36
16. Kokubu S, Eddinger KA, Nguyen TM, Huerta-Esquivel LL, Yamaguchi S, Schiller PW, Yaksh TL: Characterization of the antinociceptive effects of intrathecal DALDA peptides following bolus intrathecal delivery. Scand J Pain 2019; 19:193–206
17. Stevens CW, Yaksh TL: Spinal action of dermorphin, an extremely potent opioid peptide from frog skin. Brain Res 1986; 385:300–4
18. Schiller PW, Nguyen TM, Berezowska I, Dupuis S, Weltrowska G, Chung NN, Lemieux C: Synthesis and *in vitro* opioid activity profiles of DALDA analogues. Eur J Med Chem 2000; 35:895–901
19. Zhao GM, Qian X, Schiller PW, Szeto HH: Comparison of [Dmt1]DALDA and DAMGO in binding and G protein activation at mu, delta, and kappa opioid receptors. J Pharmacol Exp Ther 2003; 307:947–54
20. Dirig DM, Salami A, Rathbun ML, Ozaki GT, Yaksh TL: Characterization of variables defining hindpaw withdrawal latency evoked by radiant thermal stimuli. J Neurosci Methods 1997; 76:183–91
21. Wolman M, Kasten FH: Polarized light microscopy in the study of the molecular structure of collagen and reticulin. Histochemistry 1986; 85:41–9
22. Lattouf R, Younes R, Lutomski D, Naaman N, Godeau G, Senni K, Changotade S: Picrosirius red staining: A useful tool to appraise collagen networks in normal and pathological tissues. J Histochem Cytochem 2014; 62:751–8
23. Kirshenbaum AS, Akin C, Wu Y, Rottem M, Goff JP, Beaven MA, Rao VK, Metcalfe DD: Characterization of novel stem cell factor responsive human mast cell lines LAD 1 and 2 established from a patient with mast cell sarcoma/leukemia; activation following aggregation of FcepsilonRI or FcgammaRI. Leuk Res 2003; 27:677–82
24. Rådinger M, Jensen BM, Kuehn HS, Kirshenbaum A, Gilfillan AM: Generation, isolation, and maintenance of human mast cells and mast cell lines derived from peripheral blood or cord blood. Curr Protoc Immunol 2010; Chapter 7:Unit 7.37
25. Schick B, Austen KF: Modulation of chymase-mediated rat serosal mast cell degranulation by trypsin or diisopropyl fluorophosphate. Immunology 1989; 66:434–8
26. Rothschild AM: Mechanisms of histamine release by compound 48-80. Br J Pharmacol 1970; 38:253–62
27. Jordan M, Schallhorn A, Wurm FM: Transfecting mammalian cells: Optimization of critical parameters affecting calcium-phosphate precipitate formation. Nucleic Acids Res 1996; 24:596–601
28. Kroeze WK, Sassano MF, Huang XP, Lansu K, McCorvy JD, Giguère PM, Sciaky N, Roth BL: PRESTO-Tango as an open-source resource for interrogation of the druggable human GPCRome. Nat Struct Mol Biol 2015; 22:362–9
29. Stevens CW, Yaksh TL: Potency of infused spinal antinociceptive agents is inversely related to magnitude of tolerance after continuous infusion. J Pharmacol Exp Ther 1989; 250:1–8

30. Stevens CW, Yaksh TL: Time course characteristics of tolerance development to continuously infused antinociceptive agents in rat spinal cord. J Pharmacol Exp Ther 1989; 251:216–23
31. Zuo Z: The role of opioid receptor internalization and beta-arrestins in the development of opioid tolerance. Anesth Analg 2005; 101:728–34
32. Mori T, Kuzumaki N, Arima T, Narita M, Tateishi R, Kondo T, Hamada Y, Kuwata H, Kawata M, Yamazaki M, Sugita K, Matsuzawa A, Baba K, Yamauchi T, Higashiyama K, Nonaka M, Miyano K, Uezono Y, Narita M: Usefulness for the combination of G-protein- and β-arrestin-biased ligands of μ-opioid receptors: Prevention of antinociceptive tolerance. Mol Pain 2017; 13:1744806917740030
33. Altarifi AA, David B, Muchhala KH, Blough BE, Akbarali H, Negus SS: Effects of acute and repeated treatment with the biased μ-opioid receptor agonist TRV130 (oliceridine) on measures of antinociception, gastrointestinal function, and abuse liability in rodents. J Psychopharmacol 2017; 31:730–9
34. Hill R, Disney A, Conibear A, Sutcliffe K, Dewey W, Husbands S, Bailey C, Kelly E, Henderson G: The novel μ-opioid receptor agonist PZM21 depresses respiration and induces tolerance to antinociception. Br J Pharmacol 2018; 175:2653–61
35. Sajanti J, Majamaa K: Detection of meningeal fibrosis after subarachnoid haemorrhage by assaying procollagen propeptides in cerebrospinal fluid. J Neurol Neurosurg Psychiatry 1999; 67:185–8
36. Heula AL, Sajanti J, Majamaa K: Procollagen propeptides in chronic subdural hematoma reveal sustained dural collagen synthesis after head injury. J Neurol 2009; 256:66–71
37. Allen JW, Horais KA, Tozier NA, Wegner K, Corbeil JA, Mattrey RF, Rossi SS, Yaksh TL: Time course and role of morphine dose and concentration in intrathecal granuloma formation in dogs: A combined magnetic resonance imaging and histopathology investigation. Anesthesiology 2006; 105:581–9
38. Yaksh TL: Spinal delivery and assessment of drug safety. Fundamental Neuropathology for Pathologists and Toxicologists: Principles and Techniques 2011: 451–462
39. Lehmberg J, Scheiwe C, Spreer J, van Velthoven V: Late bacterial granuloma at an intrathecal drug delivery catheter. Acta Neurochir (Wien) 2006; 148:899–901; discussion 901
40. Deer TR, Pope JE, Hayek SM, Lamer TJ, Veizi IE, Erdek M, Wallace MS, Grider JS, Levy RM, Prager J, Rosen SM, Saulino M, Yaksh TL, De Andres JA, Abejon Gonzalez D, Vesper J, Schu S, Simpson B, Mekhail N: The Polyanalgesic Consensus Conference (PACC): Recommendations for intrathecal drug delivery: Guidance for improving safety and mitigating risks. Neuromodulation 2017; 20: 155–176
41. Emami A, Tepper J, Short B, Yaksh TL, Bendele AM, Ramani T, Cisternas AF, Chang JH, Mellon RD: Toxicology evaluation of drugs administered via uncommon routes: Intranasal, intraocular, intrathecal/intraspinal, and intra-articular. Int J Toxicol 2018; 37:4–27
42. Manglik A, Lin H, Aryal DK, McCorvy JD, Dengler D, Corder G, Levit A, Kling RC, Bernat V, Hübner H, Huang XP, Sassano MF, Giguère PM, Löber S, Da Duan, Scherrer G, Kobilka BK, Gmeiner P, Roth BL, Shoichet BK: Structure-based discovery of opioid analgesics with reduced side effects. Nature 2016; 537:185–90
43. Karhu T, Akiyama K, Vuolteenaho O, Bergmann U, Naito T, Tatemoto K, Herzig KH: Mast cell degranulation via MRGPRX2 by isolated human albumin fragments. Biochim Biophys Acta Gen Subj 2017; 1861(11 Pt A):2530–4
44. Smith JC, Boone BE, Opalenik SR, Williams SM, Russell SB: Gene profiling of keloid fibroblasts shows altered expression in multiple fibrosis-associated pathways. J Invest Dermatol 2008; 128:1298–310
45. Zhang T, Finn DF, Barlow JW, Walsh JJ: Mast cell stabilisers. Eur J Pharmacol 2016; 778:158–68
46. Thevenot PT, Baker DW, Weng H, Sun MW, Tang L: The pivotal role of fibrocytes and mast cells in mediating fibrotic reactions to biomaterials. Biomaterials 2011; 32:8394–403
47. Avula MN, Rao AN, McGill LD, Grainger DW, Solzbacher F: Foreign body response to subcutaneous biomaterial implants in a mast cell-deficient Kit(w-Sh) murine model. Acta Biomater 2014; 10:1856–63
48. Akers IA, Parsons M, Hill MR, Hollenberg MD, Sanjar S, Laurent GJ, McAnulty RJ: Mast cell tryptase stimulates human lung fibroblast proliferation via protease-activated receptor-2. Am J Physiol Lung Cell Mol Physiol 2000; 278:L193–201
49. Gruber BL, Kew RR, Jelaska A, Marchese MJ, Garlick J, Ren S, Schwartz LB, Korn JH: Human mast cells activate fibroblasts: tryptase is a fibrogenic factor stimulating collagen messenger ribonucleic acid synthesis and fibroblast chemotaxis. J Immunol 1997; 158:2310–7
50. Chen L, Schrementi ME, Ranzer MJ, Wilgus TA, DiPietro LA: Blockade of mast cell activation reduces cutaneous scar formation. PLoS One 2014; 9:e85226
51. Kim AJ, Basu S, Glass C, Ross EL, Agar N, He Q, Calligaris D: Unique intradural inflammatory mass containing precipitated morphine: Confirmatory analysis by LESA-MS and MALDI-MS. Pain Pract 2018; 18:889–94
52. Rijsdijk M, van Wijck AJ, Kalkman CJ, Meulenhoff PC, Grafe MR, Steinauer J, Yaksh TL: Safety assessment and pharmacokinetics of intrathecal methylprednisolone acetate in dogs. Anesthesiology 2012; 116:170–81
53. WISE BL: The reaction of the brain, spinal cord, and peripheral nerves to talc and starch glove powders. Ann Surg 1955; 142:967–72